



CHORUS

This is the accepted manuscript made available via CHORUS. The article has been published as:

Higher-Order Nonlinearities Revisited and Their Effect on Harmonic Generation

Darshana L. Weerawarne, Xiaohui Gao, Alexander L. Gaeta, and Bonggu Shim

Phys. Rev. Lett. **114**, 093901 — Published 2 March 2015

DOI: [10.1103/PhysRevLett.114.093901](https://doi.org/10.1103/PhysRevLett.114.093901)

Higher-Order Nonlinearities Revisited and Their Effect on Harmonic Generation

Darshana L. Weerawarne and Bonggu Shim*

*Department of Physics, Applied Physics and Astronomy, Binghamton University,
State University of New York, Binghamton, NY 13902, USA*

Xiaohui Gao and Alexander L. Gaeta

*School of Applied and Engineering Physics,
Cornell University, Ithaca, NY 14853. USA.*

Abstract

We report on harmonic generation experiments and calculations in air to investigate the theoretical prediction of Kolesik *et al.* [Opt. Lett. **35**, 2550 (2010)] for testing the recently proposed higher-order Kerr effect (HOKE) model. Our observations show that although the fifth-order nonlinearity is non-negligible, the overall defocusing effect via the higher-order nonlinearities is sufficiently small that plasma formation should be a main defocusing mechanism in high power filamentation. We also explore cross phase modulation via optical Kerr effect, and find that the higher-order nonlinearities can significantly alter the phase matching of harmonic generation.

PACS numbers: 42.65.Jx, 42.65.Ky, 42.65.Sf

*Electronic address: `Correspondingauthor:bshim@binghamton.edu`

Since the invention of lasers 50 years ago, rapid progress in high power laser technology has enabled investigation of highly nonlinear interactions of light with matter. Propagation of ultrashort laser pulses in matter universally involves exotic nonlinear phenomena such as the optical Kerr effect, plasma generation, and harmonic generation (HG) [1]. In particular, when a laser pulse reaches high intensity due to self-focusing via the Kerr effect, material ionization and resulting plasma defocusing have been widely believed to be a main counterbalancing mechanism against beam collapse. For example, laser filamentation, which is long-range, high intensity self-guidance of ultrashort laser pulses, has been known to be mainly due to the balance between the Kerr effect and plasma formation [2–5]. However, recent experimental [6] and theoretical [7] studies have proposed that the phenomenological higher-order (higher than third-order nonlinearity) Kerr effect rather than plasma can be a main defocusing mechanism (HOKE model), generating heated debates. In detail, as the laser intensity I increases due to self-focusing, higher-order Kerr nonlinearity (*i.e.*, $n_4 I^2 + n_6 I^3 + n_8 I^4 + \dots$) with large negative higher-order coefficients (*e.g.*, $n_4 < 0$ in [6, 7]) becomes important even at intensities below the threshold of plasma formation. As a result, the nonlinear index becomes negative and the transition from self-focusing to defocusing occurs with negligible plasma formation. Numerous experimental and theoretical studies refuting or corroborating this HOKE model have been followed [8, 9].

Recently Kolesik *et al.* [10] proposed a HG experiment to test the HOKE model that if the large negative higher-order nonlinearities are present in air, fifth-harmonic (FH) signals (energy) can be comparable to third-harmonic (TH) signals (energy) from 1.3- μm driving lasers. As a comparison, FH signals are much smaller than TH signals for the standard (plasma) model by assuming that the fifth and higher-order nonlinearities are negligible and thus FH signals are generated only by the cascaded process via $\chi^{(3)}(5\omega = 3\omega + \omega + \omega)$. Although several experiments for TH and FH generation [11–13] have been performed to verify this prediction, conclusions were different under different experimental conditions and there are more studies in favor of the HOKE model, which is contrary to the direct plasma [14] and transient-index measurements [8, 15] in favor of the standard plasma model. For the harmonic-generation study refuting the HOKE model, Ariunbold *et al.* [12] measured TH and FH signals by tightly focusing 2.2 μm beams in air. The quantity representative of the ratio of the FH energy to the TH energy defined by FH/TH was 2×10^{-4} , which was in agreement with the standard plasma model. However, the experiment was performed with

a fixed energy and the nominal peak intensity at the focus might be larger ($I > 5 \times 10^{14}$ W/cm²) than those used in the simulation ($I < 1 \times 10^{14}$ W/cm²) so that the result could not be directly compared with the theoretical calculation. For the harmonic-generation studies supporting the HOKE model, Béjot *et al.* [16] showed that the large fifth harmonic signals previously measured by Kosma *et al.* [17] can be explained by the HOKE model. Although the peak intensities used were comparable to those in the calculation by Kolesik *et al.* [10], direct comparison was not possible due to differences in the harmonic generation length. Recently a harmonic-generation experiment in air was carried out by tightly focusing 2- μ m laser beams in air with varying laser intensities [13]. The FH/TH even exceeded 0.2 so that the result was in favor of the HOKE model. However, the tight focusing geometry and resulting high intensities were different than the parameters used in the simulation. For the weaker higher-order nonlinearities, Ni *et al.* [11] performed TH and FH measurements in a narrow (2 mm) gas cell to minimize any nonlinear propagation effects. It was shown that the dependence of harmonic signals on gas pressure follows the direct HG process instead of the cascaded process suggesting that a small fifth-order nonlinearity should be present but itself is not large enough to arrest self-focusing.

In this Letter, we present TH and FH measurements in air to test the HOKE model under conditions that closely match simulation parameters used in Kolesik *et al.* [10]. When the harmonic driving pulses are focused in air generating TH and FH signals, the measured maximum FH/TH is about 0.003, which is larger than that predicted by the standard model calculation considering only cascaded FH generation and smaller than that predicted by the HOKE model. Our calculations considering proper phase matching show that although the *negative* fifth-order Kerr nonlinearity in air may be present, the overall defocusing effect via the higher-order nonlinearities should be much smaller than the original measurement [6]. Therefore, the nonlinear index transition from self-focusing to defocusing should occur at intensities in which plasma effects dominate, which is consistent with the previous studies [11, 18]. Furthermore, we find that the Kerr effect including the higher-order nonlinearities can play an important role on HG via phase matching contributed by cross phase modulation. This effect has, to the best of our knowledge, not been studied thoroughly and needs systematic investigation for efficient HG in UV and soft x-ray wavelengths using media with negligible or small fractions of ionization [19].

In our experiments, 1.33- μ m, 4-mm diameter, 55-fs FWHM laser pulses from an optical

parametric amplifier (OPA) that is pumped by 1-kHz, 800-nm, 45-fs Ti:Sapphire laser pulses are focused in air using a 15-cm focal length (f) lens. The laser input energy E is varied from $18 \mu\text{J}$ to $\sim 160 \mu\text{J}$ using a combination of a thin linear polarizer and a half-wave plate. For the highest energy ($\gtrsim 200 \mu\text{J}$), we simply remove the thin linear polarizer of which the maximum energy throughput is around 80 %. First, we measure mode profiles near the geometrical focus using imaging lenses and an infrared camera (Ophir Pyrocam) to characterize beam sizes of the focused laser beam and check any nonlinear propagation effects. The measured modes are fitted using superGaussian profiles with the Gaussian order as one of the fitting parameters to determine $1/e^2$ radii. Figure 1(a) shows that the minimum radius is about $50 \mu\text{m}$ and propagation effects such as self-focusing and defocusing are minimal except self-focusing for the highest energy ($\sim 210 \mu\text{J}$). The estimated error is $\pm 6 \mu\text{m}$ due to imaging resolutions. Therefore we have similar input beam parameters with those in Ref. [10] ($1.33\text{-}\mu\text{m}$, 50-fs FWHM, $50 \mu\text{m}$ focused radius, $E \leq 230 \mu\text{J}$) and direct comparison between experiments and simulations is possible.

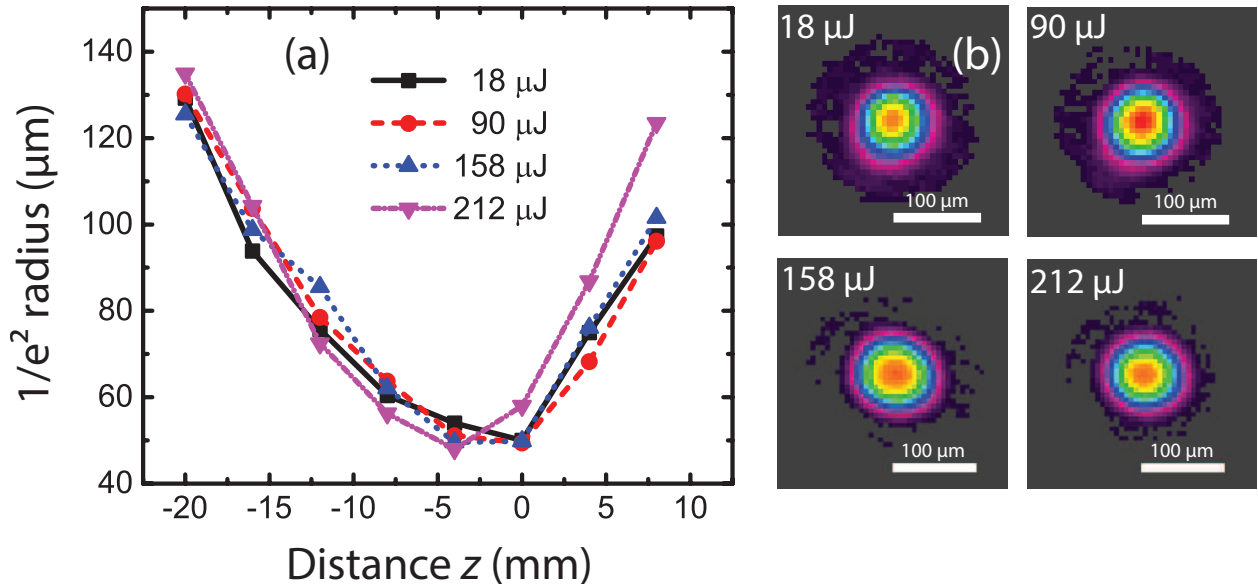


FIG. 1: (Color online) (a) Fundamental mode $1/e^2$ radius vs. propagation distance for different energies when the input beam is focused by an $f = 15$ cm lens. Here we define $z = 0$ where the beam of the minimum energy ($18 \mu\text{J}$) is focused with the smallest size and the - (+) sign indicates before (after) the geometrical focus. (b) Examples of mode profiles at $z = 0$ for different energies.

TH (~ 443 nm) and FH (~ 266 nm) signals from air with 15-cm lens are measured using

an $f = 5$ cm Al collimation mirror which is 5-cm away from the geometrical focus [square in Fig. 2(a)]. However, harmonic signals may be generated even after collimation since the Al mirror reflects most of fundamental and harmonic beams and may vary depending on the distance from the geometrical focus due to the Gouy phase shift [20]. Thus we also measure TH and FH signals using plane harmonic mirrors that reflect only TH or FH signals and a fused silica collimation lens at different distances from the focus (4, 5, and 6 cm) [open symbols in Fig. 2(a)]. The results are comparable to that using the Al mirror and the Guoy phase effect is not visible. Due to supercontinuum generation and potential harmonic generation from mirror substrates and damage, we cannot position harmonic mirrors closer than 4 cm from the focus. After the collimated signals are spatially separated by a grating with known reflection efficiencies, a calibrated photo-multiplier tube (PMT) with spectral and neutral density filters measures harmonic energies. More details about the harmonic detection setup are described in the Supplemental Material [21]. The measured FH/TH for 15-cm lens is ≤ 0.003 . Although the ratio is much closer to the standard model, it is still one-order of magnitude larger than the standard model calculation by Kolesik *et al.* [10] in which the fifth-order nonlinearity $\chi^{(5)}$ is ignored and the generated FH is only from the cascaded $\chi^{(3)}$ effects. Therefore, the measured FH signals which are larger than those for the standard model calculation should be due to non-negligible $\chi^{(5)}$. The conversion efficiencies for 15-cm lens are $< 5 \times 10^{-5}$ for TH signals, which is consistent with other measurements with similar energies [24] and $< 2 \times 10^{-7}$ for FH signals. Although TH efficiency is smaller than the simulation ($< 10^{-3}$), as Ref. [10] indicated, the individual harmonic efficiency in simulations can be affected by systematic deviations caused by parameter uncertainties. Therefore, the ratio between TH and FH signals is a better parameter to test the HOKE model since it is much less susceptible to errors. For comparison, we also carry out measurements with tighter focusing geometry using an $f = 5$ cm lens and an $f = 5$ cm Al collimation mirror [circle in Fig. 2(b)]. The focused radius for 5-cm lens is estimated to be about $17 \mu\text{m}$. For 5-cm lens, FH signals are easily detectable with low input energies and the measured FH/TH is overall one order of magnitude larger than that for $f = 15$ cm due to higher intensity achieved. This result is in good agreement with the large FH/TH measured by Nath *et al.* [13] using a tight-focusing geometry. The conversion efficiencies for 5-cm lens are $< 8 \times 10^{-4}$ for TH signals and $< 2 \times 10^{-5}$ for FH signals. We also measure TH and FH spectra by focusing harmonic signals into a fiber spectrometer. As shown in Fig. 2(c), the frequency blue shift

in TH spectra for $f = 5$ cm [25] is clearly visible due to plasma generation as compared with $f = 15$ cm.

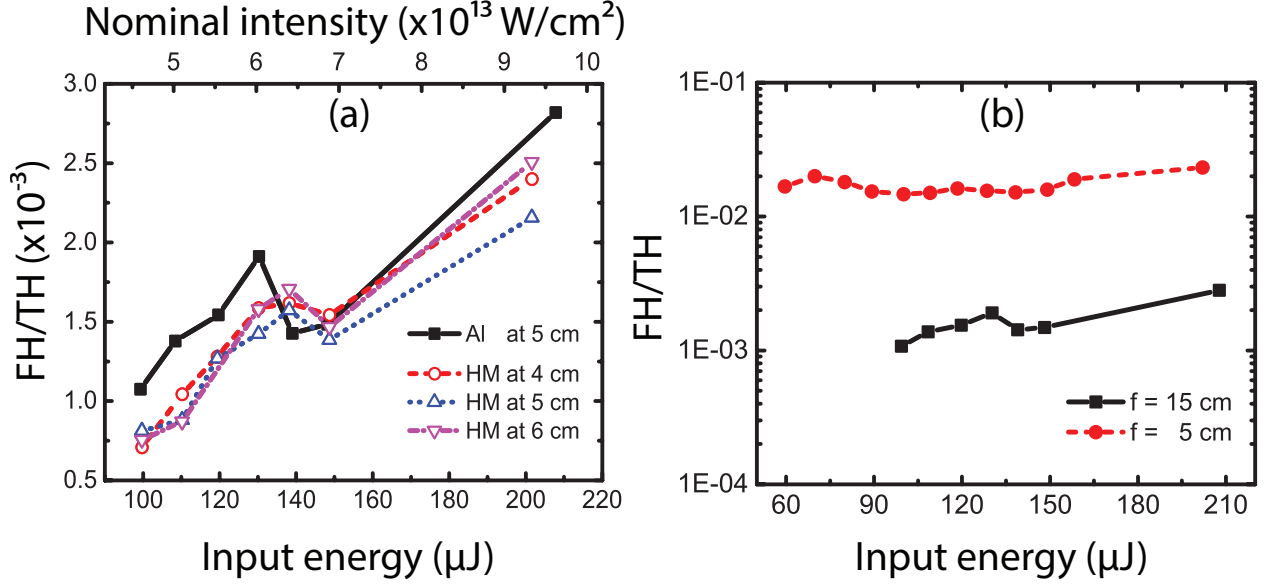


FIG. 2: (Color online) (a) Measured FH/TH from air vs. input energy for an $f = 15$ cm lens with an $f = 5$ cm Al collimation mirror (closed square), harmonic mirrors at different distances from the geometrical focus (HM: open symbols) (b) Comparison of measured FH/TH for an $f = 5$ cm lens and an $f = 15$ cm lens both with an $f = 5$ cm Al collimation mirror. (c) Examples of TH and FH spectra with $E = 150 \mu\text{J}$ for $f = 15$ cm (top) and $f = 5$ cm (bottom).

To compare with experiments, we perform numerical simulations based on the three-wave nonlinear Schrödinger equation which is an extension of the two-wave model for TH generation in air [26, 27]. The equations are given by,

$$\begin{aligned} \frac{\partial A_\omega}{\partial z} = & \frac{i}{2k_\omega} \nabla_\perp^2 A_\omega - i \frac{k_\omega''}{2} \frac{\partial^2 A_\omega}{\partial t^2} - i \frac{k_\omega}{2n_\omega} \frac{\rho}{\rho_{c\omega}} A_\omega - \frac{1}{2} \frac{\sum_k N_k W_k^\omega U_k}{|A_\omega|^2} A_\omega \\ & + i \frac{k_\omega}{n_\omega} \left(\sum_{j=1}^4 n_{2j} |A_\omega|^{2j} \right) A_\omega + i \frac{k_\omega}{n_\omega} (n_2 A_\omega^{*2} A_{3\omega} + \frac{1}{2} n_4 A_\omega^{*4} A_{5\omega} + 2n_2 A_\omega^* A_{3\omega}^* A_{5\omega}), \end{aligned} \quad (1)$$

$$\begin{aligned} \frac{\partial A_{3\omega}}{\partial z} = & \frac{i}{2k_{3\omega}} \nabla_\perp^2 A_{3\omega} - i \frac{k_{3\omega}''}{2} \frac{\partial^2 A_{3\omega}}{\partial t^2} - i \Delta k_{3\omega} A_{3\omega} - \Delta v_{g_{3\omega}} \frac{\partial A_{3\omega}}{\partial t} - i \frac{k_{3\omega}}{2n_{3\omega}} \frac{\rho}{\rho_{c_{3\omega}}} A_{3\omega} \\ & - \frac{1}{2} \frac{\sum_k N_k W_k^{3\omega} U_k}{|A_{3\omega}|^2} A_{3\omega} + i \frac{k_{3\omega}}{n_{3\omega}} \left(\sum_{j=1}^4 (j+1) n_{2j} |A_\omega|^{2j} \right) A_{3\omega} + i \frac{k_{3\omega}}{n_{3\omega}} \left(\frac{1}{3} n_2 A_\omega^3 + n_2 A_\omega^{*2} A_{5\omega} \right), \end{aligned} \quad (2)$$

$$\begin{aligned} \frac{\partial A_{5\omega}}{\partial z} = & \frac{i}{2k_{5\omega}} \nabla_{\perp}^2 A_{5\omega} - i \frac{k_{5\omega}''}{2} \frac{\partial^2 A_{5\omega}}{\partial t^2} - i \Delta k_{5\omega} A_{5\omega} - \Delta v_{g_{5\omega}, \omega} \frac{\partial A_{5\omega}}{\partial t} - i \frac{k_{5\omega}}{2n_{5\omega}} \frac{\rho}{\rho_{c_{5\omega}}} A_{5\omega} \\ & - \frac{1}{2} \frac{\sum_k N_k W_k^{5\omega} U_k}{|A_{5\omega}|^2} A_{5\omega} + i \frac{k_{5\omega}}{n_{5\omega}} \left(\sum_{j=1}^4 (j+1) n_{2j} |A_{\omega}|^{2j} \right) A_{5\omega} + i \frac{k_{5\omega}}{n_{5\omega}} \left(n_2 A_{\omega}^2 A_{3\omega} + \frac{1}{10} n_4 A_{\omega}^5 \right), \end{aligned} \quad (3)$$

where A_{ω} , $A_{3\omega}$ and $A_{5\omega}$ denote the fundamental, TH, and FH laser electric fields with the transformation $A_{3\omega} \rightarrow A_{3\omega} e^{i\Delta k_{3\omega}}$ and $A_{5\omega} \rightarrow A_{5\omega} e^{i\Delta k_{5\omega}}$, where $\Delta k_{3\omega} = 3k_{\omega} - k_{3\omega}$ and $\Delta k_{5\omega} = 5k_{\omega} - k_{5\omega}$. Here $k_{q\omega} = n_{q\omega} q k_0$ for $q = 1, 3, \text{ and } 5$, where $n_{q\omega}$ is the refractive index of the neutral air and k_0 is the vacuum wave number for the fundamental beam, represent wave vectors, z is the propagation distance, t is the retarded time for the pulse traveling at the group velocity of the fundamental beam $v_g(\omega)$, and $\Delta v_{g_{q\omega}, \omega} = [v_g^{-1}(q\omega) - v_g^{-1}(\omega)]^{-1}$, with $q = 3$ and 5 represents group velocity walk-off. The quantities ρ , $\rho_{c_{q\omega}}$, N_k , $W_k^{q\omega}$, and U_k represent the plasma density, the critical density, the neutral molecule density, the ionization rate, and the ionization energy, respectively. In Eq. (1) for the fundamental field, each term on the right side represents diffraction, dispersion, plasma defocusing, ionization absorption, and self-phase modulation (SPM) $(\sum_{j=1}^4 n_{2j} |A_{\omega}|^{2j})$, respectively, and the final three terms are harmonic back conversion terms [28]. In Eqs. (2) and (3) for the harmonic fields, each term on the right side represents diffraction, dispersion, electric field transformation ($A_{q\omega} \rightarrow A_{q\omega} e^{i\Delta k_{q\omega}}$), group delay, plasma defocusing, ionization absorption, and cross-phase modulation (XPM) $(\sum_{j=1}^4 (j+1) n_{2j} |A_{\omega}|^{2j})$, respectively and the final two terms are harmonic generation and/or wave-mixing terms [28]. We ignore negligible SPM and XPM by the TH and FH fields. In particular, $(1/3)n_2 A_{\omega}^3$, $(1/10)n_4 A_{\omega}^5$, and $n_2 A_{\omega}^2 A_{3\omega}$ represent the TH, the direct FH and the cascaded FH generation terms, respectively. For the HOKE model, we use the nonlinear coefficients in Ref. [6] (erratum) whereas for the standard model $n_2 = 1.2 \times 10^{-19} \text{ cm}^2/\text{W}$, $n_6 = n_8 = 0$ are used and n_4 is varied including sign to match the experiment [29]. For both models, plasma is generated via oxygen and nitrogen ionization in air only by the fundamental beam using the PPT model [30] and although multiphoton absorption is included for TH and FH beams, the effects are negligible. We include SPM and XPM up to the n_8 term for the full HOKE model [16] and harmonic and wave-mixing terms are based on Ref [28] neglecting terms higher than the fifth order.

To check the validity of the simple three-wave model, we first compare our calculations with the sophisticated unidirectional model by Kolesik *et al.* [10] as is shown in Fig. 3(a) for the HOKE model and the standard model with $n_4 = 0$ [STD ($n_4 = 0$)]. The standard

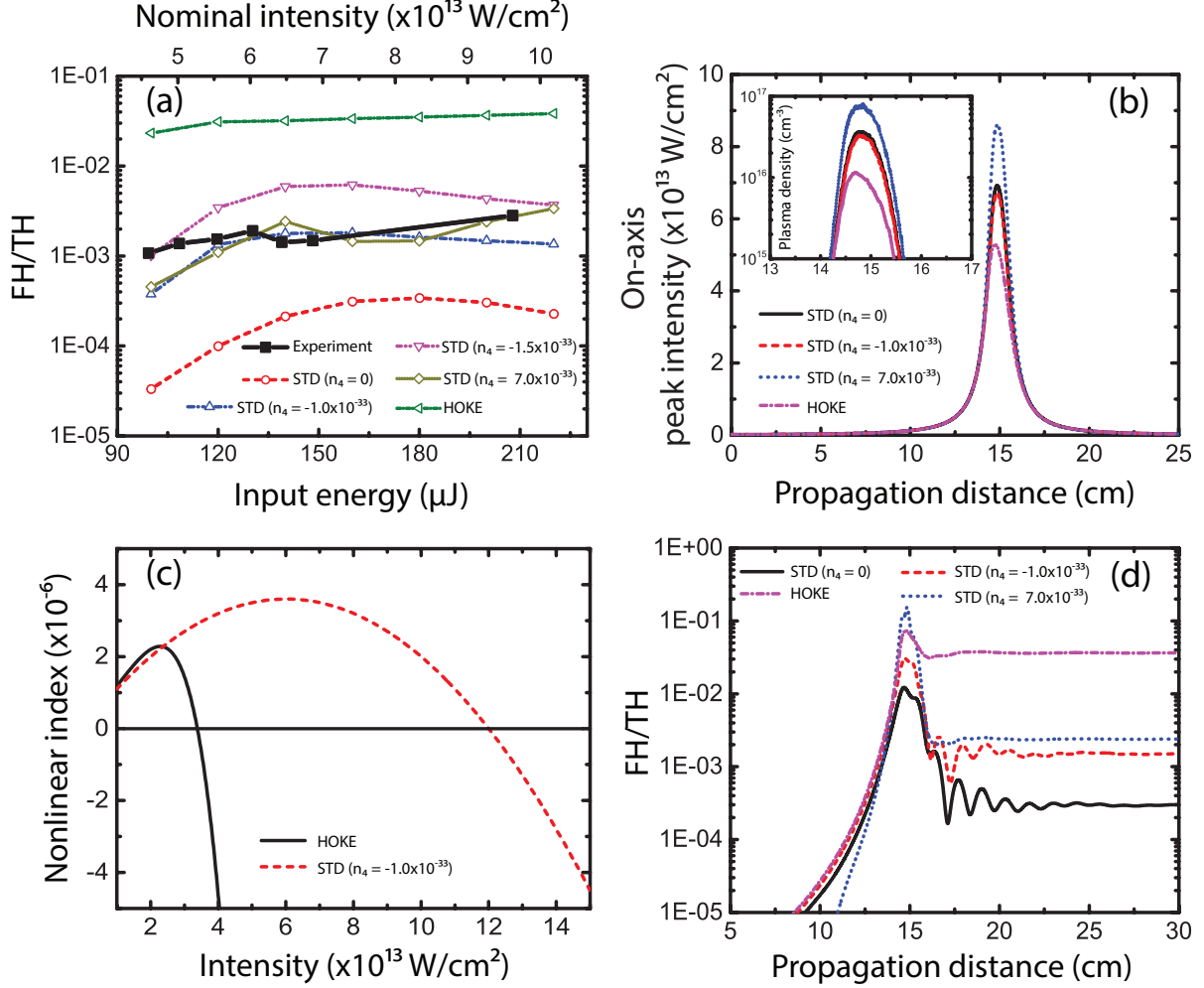


FIG. 3: (Color online) (a) Measured FH/TH (Experiment) with 15-cm lens and Al collimation mirror and calculated FH/TH (open symbols) 5-cm away from the geometrical focus using the HOKE model and the standard (STD) model with different n_4 values. (b) Calculated peak intensity vs. propagation distance for $E = 200 \mu\text{J}$. The inset shows the plasma density. The geometrical focus is at 15 cm. (c) Calculated nonlinear index vs. laser intensity for the HOKE model (black solid line) and the standard model (STD) with $n_4 = -1 \times 10^{-33} \text{ cm}^4/\text{W}^2$ (red dashed line). (d) Calculated FH/TH vs. propagation distance with 15-cm lens and $E = 200 \mu\text{J}$. The geometrical focus is at 15 cm.

model calculation is in excellent agreement with the unidirectional one. The HOKE model calculation is also in good agreement reproducing much larger FH/TH compared with the standard one despite its simplicity. Furthermore, since the n_4 value measured by Loriot *et al.* [6] has a large uncertainty [$n_4 = -(1.5 \pm 3) \times 10^{-33} \text{ cm}^4/\text{W}^2$], we perform numerical

simulations by varying n_4 within the error (see Fig. S2 in the Supplemental Material). The HOKE model with varying n_4 still produces much larger FH/TH than the standard model and the experiment. Our model enables an analysis of the role of phase matching compared with the unidirectional model. Although much larger FH/TH for the HOKE model was mainly attributed to nonlinear current effects in Ref.[10], our calculation shows that it is also strongly affected by phase mismatch for the q -th harmonic given by

$$\Delta k_{q\omega} = qk_\omega - k_{q\omega} = qk_0 \left((n_\omega - n_{q\omega}) - \frac{1}{2} \frac{q^2 - 1}{q^2} \frac{\rho}{\rho_{c\omega}} - \sum_{j=1}^4 j n_{2j} |A_\omega|^{2j} \right), \quad (4)$$

where each term represents the neutral air, plasma, and nonlinear index contributions, respectively. Since the harmonic medium is air and the confocal parameter is 1 cm, we can assume tight-focusing geometry in which positive phase mismatch is preferred for efficient HG due to the Gouy phase shift [20]. Since the air refractive index at $1.33 \mu\text{m}$ (n_ω) is smaller than those for TH and FH wavelengths ($n_{3\omega}$ and $n_{5\omega}$), both the neutral and plasma contributions are negative in Eq. 4. However, the nonlinear index contribution ($-\sum_{j=1}^4 j n_{2j} |A_\omega|^{2j}$), which is given by the difference between SPM and XPM [*i.e.*, $(\sum_{j=1}^4 n_{2j} |A_\omega|^{2j}) - (\sum_{j=1}^4 (j+1) n_{2j} |A_\omega|^{2j})$], can be positive only for the negative higher-order nonlinearities and thus can enhance harmonic generation. Nonlinear index-related phase matching will be discussed later.

Based on calculations to match the experiment [see Fig. 3(a)], large positive $n_4 = 7 \times 10^{-33} \text{ cm}^4/\text{W}^2$ and small, negative $n_4 = -1 \times 10^{-33} \text{ cm}^4/\text{W}^2$ of which magnitude is smaller than that in the HOKE model ($n_4 = -1.5 \times 10^{-33} \text{ cm}^4/\text{W}^2$) match relatively well with the experiment. The reason large positive n_4 gives similar results with small negative n_4 is because of phase matching; larger intensities for positive n_4 via enhanced self-focusing generates larger density plasma and thus poor phase matching conditions [Fig. 3(b)]. For $n_4 = 7 \times 10^{-33} \text{ cm}^4/\text{W}^2$, positive n_4 enhances only self-focusing and is therefore in favor of the standard model. As a comparison, for $n_4 = -1 \times 10^{-33} \text{ cm}^4/\text{W}^2$, a transition of the nonlinear index from self-focusing to defocusing occurs near $I = 1.2 \times 10^{14} \text{ W}/\text{cm}^2$ as compared to $3.2 \times 10^{13} \text{ W}/\text{cm}^2$ for the HOKE model [Fig. 3(c)]. For $I > 1 \times 10^{14} \text{ W}/\text{cm}^2$, ionization is significant and plasma effects should be dominant over those due to the nonlinear index. Therefore plasma should be a main defocusing mechanism in our wavelength ranges. Figure 3(d) shows the calculated FH/TH vs. propagation distance for different models with $E = 200 \mu\text{J}$. For all calculations, FH/TH reaches the maxima near the focus. As the beam

propagates further, harmonic efficiencies (not shown) and FH/TH quickly decrease due to the Gouy phase shift [20] and the ratio is stabilized after a few cm of propagation, which is consistent with the measurements using harmonic mirrors [see Fig. 2(a)]. This result also implies that short interaction lengths are preferable for the larger FH/TH, which is in good agreement with Ref. [11, 17]. More simulation details such as dispersion of the nonlinear index coefficients and differences of the nonlinear susceptibilities between harmonic generation and phase modulation [31] are described in the Supplemental Material [21]. We also discuss simulation results for the 5-cm focal length lens and the recently-proposed effect of ionization enhancement via interference between fundamental and harmonic fields [32] in the Supplemental Material [21].

Finally, we suggest that the nonlinear index contribution considering both self- and cross-phase modulation should be properly considered for HG phase matching though it has been, to the best of our knowledge, neglected or rarely discussed [33]: 1) Inclusion of XPM changes the sign of nonlinear index contribution in phase matching compared with SPM by itself. 2) Since the magnitude and the sign of nonlinear coefficients depend on frequencies, they can be large depending on frequencies of driving lasers. For example, very large nonlinear coefficients in gases due to resonance effects were measured using a mid-IR source [34] and a negative n_2 was measured with a UV wavelength [35]. 3) For mid-infrared harmonic drivers, ionization is almost negligible up to a few times of 10^{14} W/cm² intensity [19] and thus higher-order nonlinearities are potentially important.

In conclusion, we experimentally and theoretically investigate higher-order nonlinearities in air by measuring third- and fifth-harmonic signals. Our result suggests that there may be a small negative fifth-order nonlinearity but that the overall negative higher-order nonlinearity effect should be small at near-IR wavelengths such that plasma should be a main defocusing mechanism. Furthermore, cross-phase modulation with inclusion of higher-order nonlinearities could be important for HG phase-matching depending on gas species and harmonic driving wavelengths.

D. L. Weerawarne and B. Shim have been supported by SUNY Research Foundation of Binghamton University, and X. Gao and A. L. Gaeta acknowledge support from AFOSR

Grant/Award No. FA9550-10-1-0561 and DARPA through the PULSE program.

- [1] Y. R. Shen, *The Principles of Nonlinear Optics*, (Wiley, 1984).
- [2] A. Braun *et al.*, *Opt. Lett.* **20**, 73 (1995).
- [3] S. L. Chin *et al.*, *Can. J. Phys.* **83**, 863 (2005).
- [4] A. Couairon and A. Mysyrowicz, *Phys. Rep.* **441**, 47 (2007).
- [5] L. Bergé *et al.*, *Rep. Prog. Phys.* **70**, 1633 (2007).
- [6] V. Loriot, E. Hertz, O. Faucher, and B. Lavorel, *Opt. Express* **17**, 13429 (2009) and *Opt. Express* **18**, 3011 (2010).
- [7] P. BÉjot *et al.*, *Phys. Rev. Lett.* **104**, 103903 (2010).
- [8] For example O. Kosareva *et al.*, *Opt. Lett.* **36**, 1035 (2011); J. K. Wahlstrand, Y.-H. Cheng, and H. M. Milchberg, *Phys. Rev. Lett.* **109**, 113904 (2012) and references therein.
- [9] For example C. Brée *et al.*, *Phys. Rev. Lett.* **106**, 183902 (2011); P. BÉjot *et al.*, *Phys. Rev. Lett.* **106**, 243902 (2011); G. Karras *et al.*, *Phys. Rev. A* **88**, 053424 (2013) and references therein.
- [10] M. Kolesik, E. M. Wright, and J. V. Moloney, *Opt. Lett.* **35**, 2550 (2010).
- [11] J. Ni *et al.*, *Phys. Rev. A* **84**, 063846 (2011).
- [12] G. O. Ariunbold, P. Polynkin, and J. V. Moloney, *Opt. Express* **20**, 1662 (2012).
- [13] A. Nath *et al.*, *Opt. Lett.* **38**, 2560 (2013).
- [14] Y.-H. Chen *et al.*, *Phys. Rev. Lett.* **105**, 215005 (2010); P. Polynkin *et al.*, *Phys. Rev. Lett.* **106**, 153902 (2011) and B. Zhou *et al.*, *Phys. Rev. Lett.* **106**, 255002 (2011).
- [15] J. K. Wahlstrand *et al.*, *Phys. Rev. Lett.* **107**, 103901 (2011); J. H. Odnor *et al.*, *Phys. Rev. Lett.* **109**, 065003 (2012) and reference therein.
- [16] P. BÉjot *et al.*, *Opt. Lett.* **36**, 828 (2011).
- [17] K. Kosma *et al.*, *Opt. Lett.* **33**, 723 (2008).
- [18] A. Teleki, E. M. Wright, and M. Kolesik, *Phys. Rev. A* **82**, 065801 (2010).
- [19] For example E. J. Takahashi *et al.*, *Phys. Rev. Lett.* **101**, 253901 (2008); T. Popmintchev *et al.*, *Science* **336**, 1287 (2012); K. Hong *et al.*, *Opt. Lett.* **39**, 3145 (2014).
- [20] R. W. Boyd, *Nonlinear Optics*, (Academic Press, 2008).
- [21] See Supplemental Material, which includes Refs.[22, 23], for more experimental and simulation

details.

- [22] G. Karras *et al.*, Phys. Rev. A **88**, 053424 (2013).
- [23] N. Andreev *et al.*, Sov. Phys. JETP **97**, 554 (2003).
- [24] H. Xiong *et al.*, Phys. Rev. A **77**, 043802 (2008).
- [25] C. W. Siders *et al.*, J. Opt. Soc. Am. B **13**, 330 (1996).
- [26] N. Aközbeke *et al.*, Phys. Rev. Lett. **89**, 143901 (2002).
- [27] Y. Liu *et al.*, Opt. Commun. **284**, 4706 (2011).
- [28] J. F. Reintjes, *Nonlinear Optical Parametric Processes in Liquids and Gases* (Academic Press, 1984).
- [29] Although we use the term *standard model*, note that it is not a truly standard model if n_4 is large and negative so that the nonlinear index transition occurs at intensities below the threshold of plasma formation.
- [30] A. M. Perelemov, V. S. Popov, and M. V. Terent'ev, Sov. Phys. JETP **23**, 924 (1996).
- [31] K. Schuh *et al.*, Opt. Lett. **39**, 5086 (2014).
- [32] P. Béjot *et al.*, Phys. Rev. Lett. **112**, 203902 (2014).
- [33] n_2I induced phase matching effects for TH generation in gas and air are discussed, for example, in N. I. Koroteev and A. M. Zheltikov, Appl. Phys. B **67**, 53 (1998) and R. A. Ganeev *et al.*, App. Opt. **45**, 748 (2006).
- [34] D. Kartashov *et al.*, Opt. Lett. **37**, 2268 (2012).
- [35] R. H. Lehmborg *et al.*, Opt. Commun. **121**, 78 (1995).